Metamaterial-enhanced four-port MIMO antenna for 5G communications at 28/38 GHz

Remili Fatima[1], Bouttout Farid[1], Djellid Asma[2]
[1]ETA laboratory, Department of Electronic, Faculty of Technology, University of Mohamed El Bachir El Ibrahimi-Bordj Bou Arréridj, Bordj Bou Arréridj, Algeria
[2]Department of Electronic, Faculty of Technology, University of Mouhamed Boudiaf M'Sila, M'Sila, Algeria

Article Info

Article history:

Received Jun 23, 2025
Revised Sep 25, 2025
Accepted Oct 19, 2025

Keywords:

Electromagnetic software
Equivalent circuit
MmWave technology
Multiple-in multiple-out antenna
Planar antenna

ABSTRACT

This work presents a novel compact four-port multiple-in multiple-out (MIMO) antenna enhanced with metamaterial unit cells for 5G millimeter-wave (mmWave) applications at 28 and 38 GHz. Compact MIMO antennas at mmWave bands often suffer from high mutual coupling, which degrades isolation and diversity performance. To address this, the proposed design integrates metamaterial loading around each radiating element to effectively suppress coupling, enhance isolation, and improve overall efficiency. The antenna, measuring 27×27×0.8 mm³, is implemented on a flexible FR4_epoxy substrate (εr=4.4), enabling compatibility with portable and embedded devices. Full-wave simulations performed in both ANSYS high-frequency structure simulator (HFSS) and computer simulation technology (CST) studio suite confirm the effectiveness of the approach, achieving an exceptionally low envelope correlation coefficient (ECC) (0.0001), a fivefold reduction in channel capacity loss (CCL), and a wide impedance bandwidth of 25.90–34.93 GHz with |S11| below −10 dB in both operating bands. The design also exhibits stable directional gain and low sidelobes. Compared with recent compact MIMO antennas reported in the literature, the proposed configuration offers significantly improved isolation, bandwidth, and mechanical flexibility. These features make it a strong candidate for integration into high-capacity 5G modules, portable terminals, and compact internet of things (IoT) communication systems.

Corresponding Author:

Remili Fatima
ETA laboratory, Department of Electronic, Faculty of Technology
University of Mohamed El Bachir El Ibrahimi-Bordj Bou Arréridj
Bordj Bou Arréridj, Algeria
Email: fatima.remili@univ-bba.dz

1. INTRODUCTION

According to recent statistics from the International Telecommunication Union (ITU), the number of internet users worldwide exceeded 5.35 billion in January 2024, reflecting a growing demand for wireless communication systems capable of delivering high data rates, low latency, and robust reliability [1]. Fifth-generation (5G) networks address this demand by offering substantial improvements in spectral efficiency and beamforming over previous generations [2], [3]. To further support 5G deployment, the federal communications commission (FCC) has increased the allocated spectrum to 400 MHz, compared to 100 MHz for typical 4G deployments [4], [5].

In millimeter-wave (mmWave) systems, compact multiple-input multiple-output (MIMO) antennas are critical for achieving high capacity and dense connectivity. However, their closely spaced radiating elements often suffer from strong mutual coupling, which degrades isolation, increases correlation, and reduces diversity performance [6]-[8]. Metamaterials-engineered electromagnetic structures offer an attractive solution to this challenge, as they provide a passive, compact, and frequency-selective approach to suppress surface currents and enhance isolation without requiring complex circuitry [8], [9].

This work presents a compact four-element mmWave MIMO antenna in which metamaterial unit cells are strategically integrated around each radiating element to mitigate coupling while preserving a small footprint [10], [11]. The design is evaluated through reflection coefficient S_{11}, transmission coefficient S_{21}, and envelope correlation coefficient (ECC) to verify its suitability for next-generation wireless systems [12], [13]. The main contributions of this work are: i) a compact four-element mmWave MIMO antenna integrated with metamaterial cells for improved isolation; ii) comprehensive performance analysis using ECC and channel capacity loss (CCL) metrics; and iii) validation of the proposed design throughhigh-frequency structure simulator (HFSS) / computer simulation technology (CST) simulations and equivalent circuit modeling.

2. METHOD

The proposed antenna was designed through six fundamental steps, as illustrated in Figure 1. In the first step, the FR4 substrate with a thickness of 0.8 mm and a dielectric constant of 4.4 was placed. In the second step, a feed line with a copper circle on the top side was introduced. In the third step, the circle was modified into a crescent shape to enhance the antenna characteristics. In the fourth step, a small copper circle was added at the center of the crescent to improve electromagnetic coupling. In the fifth step, the bottom side of the antenna was covered with a full copper layer to reduce losses and improve radiation performance. Finally, in the sixth step, a square slot was etched from the copper layer on the back side to improve impedance matching and widen the bandwidth.

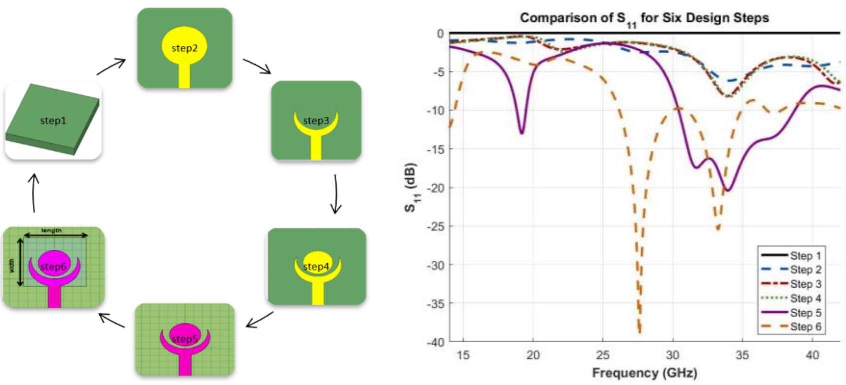

(a) (b)

Figure 1. Design evolution and performance of the proposed antenna; (a) six design stages and (b) simulated reflection coefficients for each stage

Following these design stages, the optimized antenna structure was obtained. Figure 1(a) illustrates the six design stages of the proposed antenna, showing the evolution from the initial to the optimized configuration. The gain values at each stage are presented in Table 1, while the simulated reflection coefficient S_{11} results are illustrated in Figure 1(b) to highlight the impact of these successive modifications on the antenna performance. In Figures 2(a) and (b), the simulated S-parameter results are illustrated for the parametric variations of the length and width of the etched square slot on the ground plane, respectively. The results demonstrate that the antenna maintains a stable resonance with only minor frequency shifts under these dimensional changes, indicating that the proposed structure exhibits robust impedance matching and reliable performance. This parametric study further validates the choice of the optimized dimensions and confirms the robustness of the antenna design.

To enhance the antenna performance, a conventional. unit cell was employed as a metamaterial inclusion. In Figure 3(a), the proposed split-ring resonator (SRR) cell is shown, while Figure 3(b) illustrates its extracted electromagnetic characteristics. The SRR was directly adopted from the standard HFSS library without any geometric modifications and was printed on the same FR4 substrate ($\varepsilon r = 4.4$, $thickness = 0.8$ mm) used for the antenna. The SRR consists of two concentric metallic rings with narrow splits, enabling strong resonant behavior due to the capacitive gap and the inductive loop, which helps suppress surface wave propagation and consequently improves isolation and bandwidth. The unit cell was simulated under periodic boundary conditions using wave ports to extract its S-parameters, from which the effective permittivity (εeff) and permeability (μeff) were retrieved using the standard method [7], [10]. In addition, the dispersion diagram of the SRR was obtained to verify the stopband characteristics within the 28–38 GHz range, thereby justifying the integration of SRR arrays into the antenna ground plane to achieve higher gain, improved impedance matching, and reduced mutual coupling.

Table 1. Simulated gain for the six design steps

Variable	Gain
Step 1	8.1
Step 2	7.3
Step 3	6.8
Step 4	6.4
Step 5	4.3
Step 6	3.5

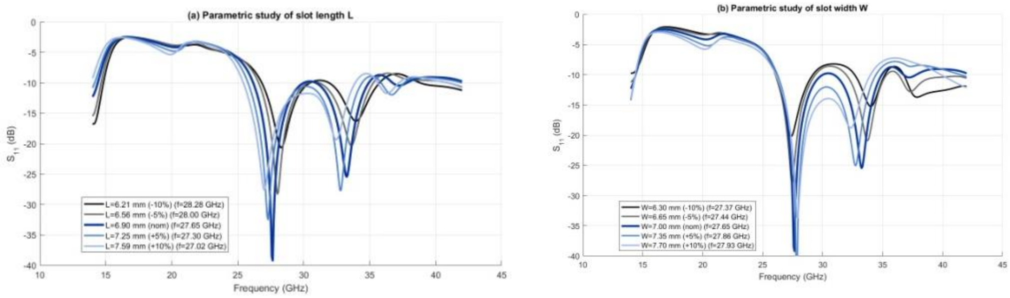

(a) (b)

Figure 2. Simulated reflection coefficients of the proposed antenna under different geometrical variations; (a) variation of the slot length and (b) variation of the slot width

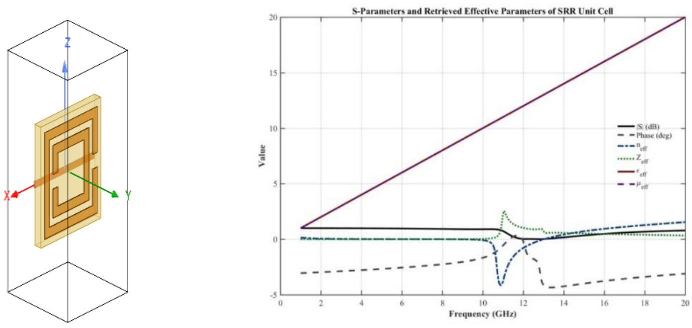

(a) (b)

Figure 3. Structure and electromagnetic characterization of the proposed SRR unit cell; (a) geometry of the unit cell and (b) retrieved electromagnetic parameters

For a clearer view of the structural configuration, Figures 4(a) and (b) show the front and back views of the proposed MIMO antenna element with integrated metamaterial cells, while Figures 4(c) and (d) present the corresponding views of the antenna without metamaterial integration. This comparative illustration highlights the physical differences between the simulated design and the fabricated prototype, as well as the placement and impact of the metamaterial inclusions within the antenna geometry. Moreover, the fabricated prototype is included to demonstrate the feasibility of implementing the proposed antenna structure. Although experimental measurements could not be performed, the fabrication confirms that the antenna can be practically realized, supporting the validity of the simulation-based design.

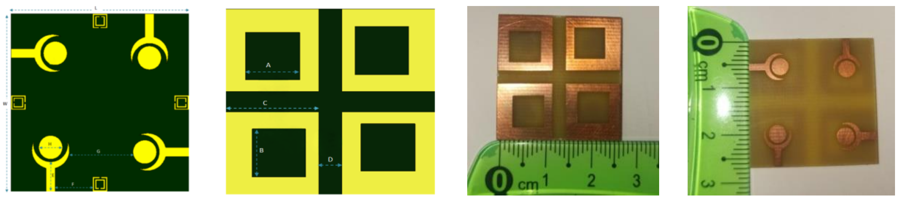

(a) (b) (c) (d)

Figure 4. Proposed and fabricated MIMO antenna element designs with and without metamaterial unit cells; (a) proposed design – front view, (b) proposed design – back view, (c) fabricated design without metamaterials – front view, and (d) fabricated design without metamaterials – back view

The proposed MIMO antenna consists of four orthogonally arranged radiating elements in a square configuration, designed to operate at 28 GHz and 38 GHz. It is implemented on a low-cost FR4_epoxy substrate with a relative permittivity (εr) of 4.4 and a thickness of 0.8 mm. Metamaterial unit cells are placed symmetrically around each patch to suppress surface currents and improve inter-element isolation. The overall geometry of the antenna is illustrated in Figure 4, and the physical dimensions are defined as: $L = 27$mm, $W = 27$ mm, $H = 1.8$ mm, $E = 3.5$ mm, $F = 5.7$ mm, $G = 9.65$ mm, $A = 7$ mm, $B = 6.9$ mm, $C = 12$ mm, and $D = 3$ mm.

3. RESULTS AND DISCUSSION

The ECC is a critical metric used to evaluate the diversity performance of MIMO antennas. Although several methods exist to compute ECC, the most common approach relies on S-parameter data, which enables a simplified mathematical formulation [14], [15]. In (1) was implemented in matrix laboratory (MATLAB) using the simulated S-parameters to calculate the ECC between antenna elements and assess the isolation characteristics of the proposed design.

$$ECC = \frac{|S_{11}*S_{12}+S_{21}*S_{22}|^2}{(1-|S_{11}|^2-|S_{21}|^2)(1-|S_{22}|^2-|S_{12}|^2)} \quad (1)$$

From the obtained results presented in Figure 5(a), it is clear that the presence of metamaterial cells significantly improves the ECC performance of the proposed MIMO antenna, where the antenna operates without metamaterial cells, the ECC values are relatively higher across the operating band. Shows the antenna with metamaterial cells, where the ECC values remain very low over the entire frequency range of 26–37 GHz, not exceeding 0.02. This improvement is especially noticeable at 28 GHz, where the ECC reaches 0.0001, confirming a strong reduction in mutual coupling and better isolation between elements. directly compares the two cases, making the difference visually evident and further demonstrating that metamaterial cells are an effective solution to reduce correlation and enhance the overall channel efficiency of the MIMO system.

CCL measures the reduction in channel capacity resulting from mutual coupling [16], [17], and correlation effects between MIMO antenna elements [18], [19]. In this work, CCL was computed in MATLAB based on the previously obtained ECC values, following standard channel capacity equations. The resulting CCL values were analyzed to evaluate the impact of metamaterial integration on system performance.

The CCL results are presented in Figure 5(b) for both configurations of the proposed MIMO antenna illustrates the case without metamaterial cells, where the CCL values are noticeably higher across the operating band, indicating stronger performance degradation due to mutual coupling, with metamaterial cells integrated, the CCL values drop significantly and remain very low over the entire frequency range of 26–37 GHz. The most notable improvement occurs near 28 GHz, where the CCL is at its minimum, confirming the effectiveness of the metamaterials in preserving channel capacity.

3.1. Equivalent circuit model

The proposed dual-band antenna was also represented as an equivalent electrical circuit composed of lumped elements (resistors (R), inductors (L), and capacitors (C)), as illustrated in Figure 6. In this model, the C represent the capacitive gaps between metallic parts of the antenna, the L account for the current paths and magnetic energy storage in the patches and feed lines, and the R model both the conductor and dielectric losses. Together, these lumped elements reproduce the antenna's input impedance characteristics at the two resonant frequencies (28 GHz and 38 GHz) [20].

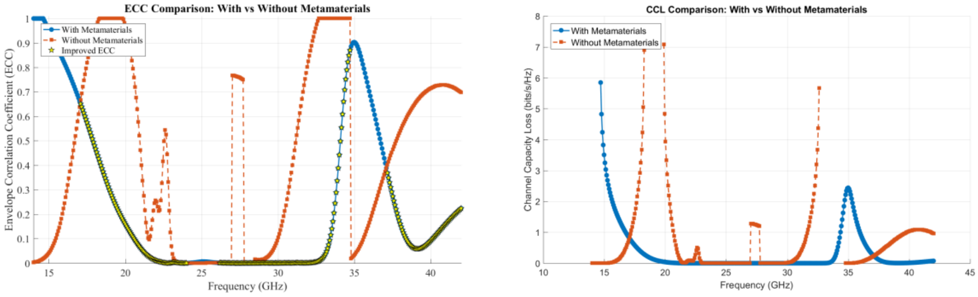

(a) (b)

Figure 5. Performance comparison of the proposed MIMO antenna with and without metamaterial unit cells; (a) ECC and (b) CCL

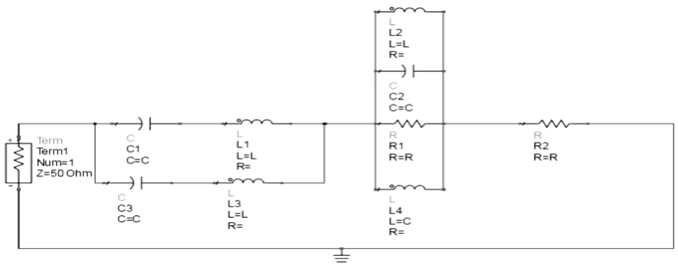

Figure 6. Equivalent circuit model for impedance matching of a dual-frequency antenna

The values of these elements were determined using analytical (2)-(6). Specifically, the resistance R is obtained from the conductor conductivity ($\sigma cond$) and the skin depth (δ), which describes ohmic loss at high frequency. The inductance L is related to the permeability of free space ($\mu 0$), the frequency (f), and the conductor dimensions (w, h), representing the magnetic energy stored in the current path. The capacitance C is derived from the effective permittivity ($\varepsilon 0, \varepsilon r$) and the separation distance d between conductors, reflecting the electric field energy in the gaps. These relations ensure that the lumped circuit parameters are directly connected to the physical properties of the antenna [21], [22].

The circuit model was implemented in advanced design system (ADS), where the dual-band behavior is reproduced by two resonant LC branches: the first branch is responsible for resonance at 28 GHz, while the second resonates at 38 GHz. By tuning the lumped values, the ADS response was adjusted to match the simulated S-parameters. Although detailed ADS schematics are not included here, the equivalent circuit provides valuable analytical insight into how the antenna stores and dissipates energy, how impedance matching is achieved, and how the two operating frequencies are generated. This representation complements the full-wave electromagnetic simulations and validates the theoretical design.

$$R = \frac{1}{\omega \cdot \sigma_{cond} \cdot \delta} \tag{2}$$

$$\delta = \sqrt{\frac{1}{\pi . f . \mu_0 . \sigma_{cond}}} \tag{3}$$

$$L = \frac{\mu_0}{2\pi} . ln(\frac{2h}{\omega}) \tag{4}$$

$$C = \frac{\varepsilon_r . \varepsilon_0 . \omega}{d} \tag{5}$$

where:
ω = width of the transmission line (in meters)
σ_{cond} = conductivity of the conductive material (in Siemens per meter S/m)
δ = skin depth
f = frequency (in Hz)

μ_0 = permeability of free space ($4\pi\times10-7$H/m)
h = height of the substrate or distance between the conductor and the ground plane (in meters)
εr = relative permittivity of the dielectric material
ε_0 = permittivity of free space ($8.854\times10-12$ F/m)
d = distance between the conductor and the ground plane (in meters)

$$Z(f) = R + jwL - \frac{1}{jwC} \tag{6}$$

The results shown below are for the MIMO antenna with and without meta cells, which were intended to improve its properties, and that is what we obtained. The idea is based on the presence of cells surrounding the antenna elements to reduce interference and improve isolation. We were able to manufacture the antenna but could not conduct experimental measurements due to the lack of a power supply system. To give the work scientific credibility, we replaced the experimental measurements with advanced simulators. HFSS and CST showed great agreement, especially since the simulation was conducted in the presence and absence of cells, where the antenna parameters were compared, with a very noticeable improvement when using cells, as is clear in the Figure 7. Furthermore, Table 2 provides a comparative analysis between the proposed antenna and several recently reported MIMO antenna designs. As can be seen, the proposed structure achieves superior performance in terms of bandwidth, compactness, and isolation. This comparison clearly demonstrates that the integration of metamaterial unit cells significantly enhances both bandwidth and isolation, establishing the proposed design as a strong candidate for next-generation MIMO communication systems.

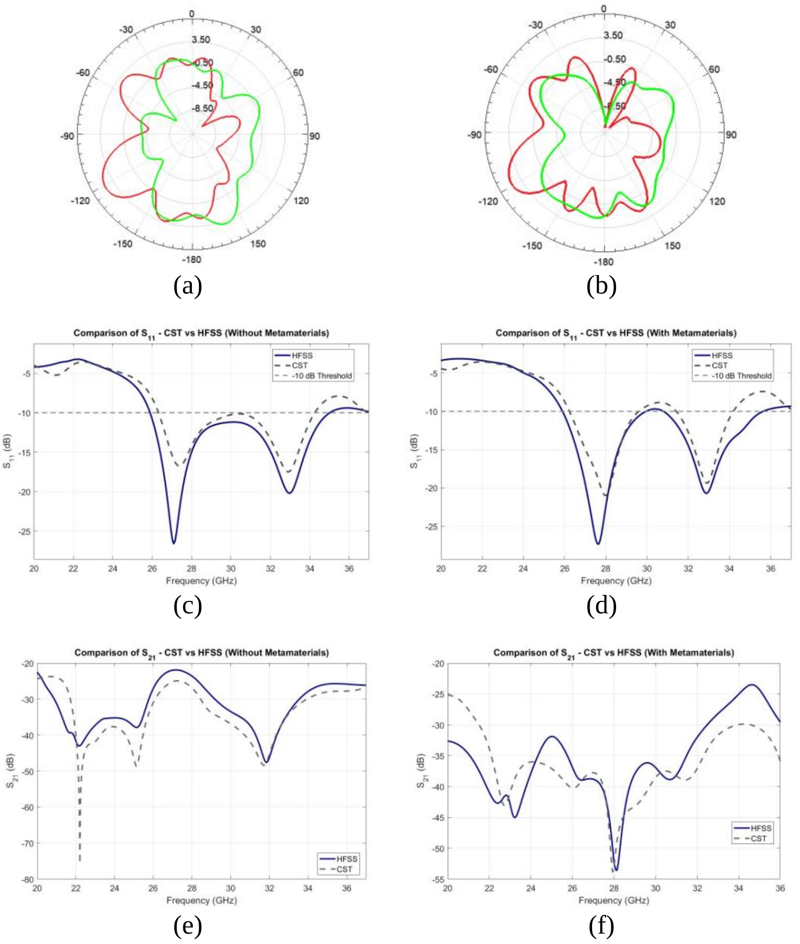

Figure 7. Simulated performance of the proposed MIMO antenna; (a) radiation patterns in E-plane, (b) radiation patterns in H-plane, (c) S_{11} responses withoutmetamaterial unit cells using HFSS and CST, (d) S_{11} responses with metamaterial unit cells using HFSS and CST, (e) S_{21} responses without metamaterial unit cells using HFSS and CST, and (f) S_{21} responses with metamaterial unit cells using HFSS and CST

Table 2. Comparison of performance metrics with other MIMO antenna designs

Ref.	Antenna size (mm _ mm)	Bandwidth in GHz	No. of elements	ECC
[19]	30.5×25.5	4.84–5	2	<0.02
[20]	25×20×0.79	27.2–28.72 36.2–42	4	0.002
[23]	6×17.37	37.471–38 34.1–39.7	2	0.0003
[24]	0.52×0.52×0.1	3.04–5.05	4	<0.006
[25]	78×50	3.3-6.3	4	0.05
This work without metamaterials	27×27×0.8	25.90–29.96 31.01–35.70	4	0.0005
This work with metamaterials	27×27×0.8	25.90–34.93 30.94–35.84	4	0.0001

Figure 7 presents the key results related to the MIMO antenna performance. The reflection coefficients remain below −10 dB within the operating bands, while the transmission coefficients demonstrate the level of isolation between the ports. Figures 7(a) and (b) displays the radiation patterns in the E-plane and H-plane, showing a well-defined main lobe with low sidelobes. Figures 7(c) and (d) compare the S_{11} responses in both cases (without and with metamaterial unit cells) based on simulations from both HFSS and CST, where the results indicate a bandwidth enhancement when the cells are added. Finally, Figures 7(e) and (f) present a comparison of the S_{21} curves, showing that the use of metamaterial unit cells improves isolation and reduces coupling between the antenna elements.

Moreover, the radiation patterns further highlight the effect of the metamaterial cells. In the absence of the unit cells, the patterns exhibit irregular lobes with noticeable side radiation, which indicates stronger coupling and reduced directivity. When the metamaterial cells are introduced, the radiation becomes more uniform, with clearer main lobes and suppressed sidelobes. This improvement reflects enhanced directivity, better port isolation, and reduced mutual coupling, thereby validating the role of metamaterials in optimizing the electromagnetic behavior of the proposed MIMO antenna. It should be noted that HFSS and CST simulations were employed due to the unavailability of measurement facilities, despite the antenna being fabricated.

The analysis of the S-parameters, particularly the significant reduction in S_{21} clearly demonstrates the improvement in isolation between the MIMO antenna elements when using the proposed metamaterial cells. This enhancement directly contributes to reducing the correlation between the antenna ports, as further confirmed by the calculated ECC and CCL values. As shown in Figure 5, the ECC of the proposed structure is less than 0.0001 at 28 GHz, which is far below the acceptable limit of 0.5 [15], [24], [25], indicating excellent diversity performance.

4. CONCLUSION

In this study, a four-element integrated MIMO antenna measuring 27×27×0.8 mm^3 is proposed for 5G (mmWave) applications at 28 and 33 GHz. The design, evaluated through full simulation using HFSS and CST software, demonstrated outstanding performance with an ECC as low as 0.0001, ensuring strong isolation and significantly reducing inter-element coupling. A prototype was fabricated, and experimental verification will be conducted in future work. Comparisons between HFSS and CST simulations showed high agreement, and analytical validations using MATLAB, along with an equivalent circuit model, confirmed the robustness of the design. These results highlight the antenna's potential for seamless integration into future 5G communication systems in the mmWave band.

FUNDING INFORMATION

Authors state no funding involved.

AUTHOR CONTRIBUTIONS STATEMENT

This journal uses the Contributor Roles Taxonomy (CRediT) to recognize individual author contributions, reduce authorship disputes, and facilitate collaboration.

Name of Author	C	M	So	Va	Fo	I	R	D	O	E	Vi	Su	P	Fu
Remili Fatima	✓	✓	✓		✓	✓		✓	✓	✓	✓		✓	
Bouttout Farid				✓		✓			✓		✓	✓	✓	
Djellid Asma				✓		✓	✓		✓		✓	✓	✓	

C : **C**onceptualization		I : **I**nvestigation		Vi : **Vi**sualization			
M : **M**ethodology		R : **R**esources		Su : **Su**pervision			
So : **So**ftware		D : **D**ata Curation		P : **P**roject administration			
Va : **Va**lidation		O : Writing -**O**riginal Draft		Fu : **Fu**nding acquisition			
Fo : **Fo**rmal analysis		E : Writing - Review &**E**diting					

CONFLICT OF INTEREST STATEMENT

Authors state no conflict of interest.

DATA AVAILABILITY

The data that support the findings of this study are available from the corresponding author, F.R., upon reasonable request.

REFERENCES

[1] T. Raj, R. Mishra, P. Kumar, and A. Kapoor, "Advances in MIMO antenna design for 5G: a comprehensive review," *Sensors*, vol. 23, no. 14, p. 6329, Jul. 2023, doi: 10.3390/s23146329.

[2] S. H. Kiani, M. Marey, H. Ș. Savci, H. Mostafa, U. Rafique, and M. A. Khan, "Dual-band multiple-element MIMO antenna system for next-generation smartphones," *Applied Sciences (Switzerland)*, vol. 12, no. 19, p. 9694, Sep. 2022, doi: 10.3390/app12199694.

[3] J. G, I. Singh, and D. K. Choudhary, "Gain and isolation improvement techniques for MIMO antenna: a compendious survey," *Results in Engineering*, vol. 25, p. 104482, Mar. 2025, doi: 10.1016/j.rineng.2025.104482.

[4] J. Du and R. A. Valenzuela, "How much spectrum is too much in millimeter wave wireless access," *IEEE Journal on Selected Areas in Communications*, vol. 35, no. 7, pp. 1444–1458, Jul. 2017, doi: 10.1109/JSAC.2017.2698859.

[5] M. A. Sufian, N. Hussain, and N. Kim, "Quasi-binomial series-fed array for performance improvement of millimeter-wave antenna for 5G MIMO applications," *Engineering Science and Technology, an International Journal*, vol. 47, p. 101548, Nov. 2023, doi: 10.1016/j.jestch.2023.101548.

[6] M. Benzaghta and K. M. Rabie, "Massive MIMO systems for 5G: A systematic mapping study on antenna design challenges and channel estimation open issues," *IET Communications*, vol. 15, no. 13, pp. 1677–1690, Aug. 2021, doi: 10.1049/cmu2.12180.

[7] M. M. Hasan *et al.*, "A compact mu-near-zero metamaterial integrated wideband high-gain MIMO antenna for 5G new radio applications," *Materials*, vol. 16, no. 4, p. 1751, Feb. 2023, doi: 10.3390/ma16041751.

[8] Z. Song, S. Zhao, S. Li, J. Chen, and Y. Xue, "High-isolation compact MIMO antenna with distributed metamaterial loading," *Progress In Electromagnetics Research M*, vol. 128, pp. 51–59, 2024, doi: 10.2528/PIERM24060507.

[9] S. K. Patel and A. Baz, "Design and measurement of a compact MIMO antenna using C-shaped metamaterial for 5G/6G wireless communication circuit," *Alexandria Engineering Journal*, vol. 118, pp. 159–173, Apr. 2025, doi: 10.1016/j.aej.2024.12.121.

[10] M. M. Hasan, M. T. Islam, T. Alam, P. Kirawanich, S. Alamri, and A. S. Alshammari, "Metamaterial loaded miniaturized extendable MIMO antenna with enhanced bandwidth, gain and isolation for 5G sub-6 GHz wireless communication systems," *Ain Shams Engineering Journal*, vol. 15, no. 12, p. 103058, Dec. 2024, doi: 10.1016/j.asej.2024.103058.

[11] M. A. Rahman, S. S. Al-Bawri, W. M. Abdulkawi, and M. T. Islam, "Miniaturized tri-band integrated microwave and millimeter-wave MIMO antenna loaded with metamaterial for 5G IoT applications," *Results in Engineering*, vol. 24, p. 103130, Dec. 2024, doi: 10.1016/j.rineng.2024.103130.

[12] W. Ali, S. Das, H. Medkour, and S. Lakrit, "Planar dual-band 27/39 GHz millimeter-wave MIMO antenna for 5G applications," *Microsystem Technologies*, vol. 27, no. 1, pp. 283–292, Jan. 2021, doi: 10.1007/s00542-020-04951-1.

[13] W. A. E. Ali, M. A. Abdelghany, and A. A. Ibrahim, "Wideband and high gain elliptically-inspired 4 × 4 MIMO antenna for millimeter wave applications," *Heliyon*, vol. 10, no. 20, p. e38697, Oct. 2024, doi: 10.1016/j.heliyon.2024.e38697.

[14] A. Omar, M. Hussein, I. J. Rajmohan, and K. Bathich, "Dual-band MIMO coplanar waveguide-fed-slot antenna for 5G communications," *Heliyon*, vol. 7, no. 4, p. e06779, Apr. 2021, doi: 10.1016/j.heliyon.2021.e06779.

[15] C. Du, F. Zhang, and R. Li, "Design of tri-band flexible CPW 4-port slot MIMO antenna for conformal 5G, WIFI 6/6E and X-band applications," *Engineering Science and Technology, an International Journal*, vol. 62, p. 101937, Feb. 2025, doi: 10.1016/j.jestch.2024.101937.

[16] K. S. Sultan and H. H. Abdullah, "Planar UWB MIMO-diversity antenna with dual notch characteristicst," *Progress In Electromagnetics Research C*, vol. 93, pp. 119–129, 2019, doi: 10.2528/pierc19031202.

[17] T. Islam, F. N. Alsunaydih, F. Alsaleem, and K. Alhassoon, "Analyzing the performance of millimeter wave MIMO antenna under different orientation of unit element," *Micromachines*, vol. 14, no. 11, p. 1975, Oct. 2023, doi: 10.3390/mi14111975.

[18] S. F. Bin Faruquee, H. Bhuiyan, M. S. Alam, S. Islam, and K. Ali, "Swarm intelligence driven inverse design of slot patterns for sub-6 GHz 5G MIMO antennas in virtual reality applications," *Engineering Science and Technology, an International Journal*, vol. 64, p. 102026, Apr. 2025, doi: 10.1016/j.jestch.2025.102026.

[19] K. Pandya, T. Upadhyaya, V. Sorathiya, U. Patel, A. Pandya, and F. A. Al-Zahrani, "Highly isolated electrically compact UWB MIMO antenna for wireless communications applications," *Results in Engineering*, vol. 24, p. 103082, Dec. 2024, doi: 10.1016/j.rineng.2024.103082.

[20] A. Baz, D. Jansari, S. P. Lavadiya, and S. K. Patel, "Miniaturized and high gain circularly slotted 4×4 MIMO antenna with diversity performance analysis for 5G/Wi-Fi/WLAN wireless communication applications," *Results in Engineering*, vol. 20, p. 101505, Dec. 2023, doi: 10.1016/j.rineng.2023.101505.

[21] A. Wajid, A. Ahmad, S. Ullah, D. Y. Choi, and F. U. Islam, "Performance analysis of wearable dual-band patch antenna based on EBG and SRR surfaces," *Sensors*, vol. 22, no. 14, p. 5208, Jul. 2022, doi: 10.3390/s22145208.

[22] N. Salim, M. J. Singh, H. Dibs, A. T. Abed, M. T. Islam, and M. S. Islam, "Comparative performance analysis of two novel design MIMO antennas for 5G and Wi-Fi 6 applications," *Results in Engineering*, vol. 25, p. 103808, Mar. 2025, doi:

10.1016/j.rineng.2024.103808.
[23] M. Mahaboob Basha, P. Pradeep, S. Gundala, and J. Syed, "Design of compact and high gain dual-band four-port MIMO antenna array for mm-wave 5G Communications," *Results in Engineering*, vol. 25, p. 104153, Mar. 2025, doi: 10.1016/j.rineng.2025.104153.
[24] O. Elalaouy, M. EL Ghzaoui, and J. Foshi, "A high-isolated wideband two-port MIMO antenna for 5G millimeter-wave applications," *Results in Engineering*, vol. 23, p. 102466, Sep. 2024, doi: 10.1016/j.rineng.2024.102466.
[25] H. R. Barua and I. A. Chowdhury, "Design and analysis of mm-wave MIMO antenna with DGS for 5G applications," *Journal of Electrical Systems and Information Technology*, vol. 12, no. 1, p. 17, Jun. 2025, doi: 10.1186/s43067-025-00212-1.

BIOGRAPHIES OF AUTHORS

Remili Fatima received the Baccalaureate degree in 2015 and the B.Sc. degree in Industrial Electronics from the University of BordjBouArréridj, Algeria, in 2018. She obtained the M.Sc. degree in Industrial Electronics from the same university in 2020. She is currently pursuing the Ph.D. degree in Electrical and Electronics Engineering at Mohamed El Bachir El Ibrahimi University, BordjBouArréridj, Algeria. In addition, she has actively participated in national and international conferences. Her research interests include industrial electronics, microstrip and MIMO antennas, metamaterials, and 5G millimeter-wave communication systems. She can be contacted at email: fatima.remili@univ-bba.dz.

Bouttout Farid received the B.Sc. and M.Sc. degrees in Electronics from the University of Constantine, Algeria, in 1994 and 1997, respectively, and the Ph.D. degree in Electronic Engineering from the University of Setif, Algeria, in 2001. He was a lecturer in Electronics at the University of Constantine (1996–2000) and an assistant professor at the University of M'sila (2000–2004). In addition, he held a three-year postdoctoral fellowship on printed antenna design for medical applications at the Commissariat à l'énergieatomique et aux énergies alternatives (CEA) and Pierre and Marie Curie University (UPMC – Paris 6), France. He is currently a professor with the Department of Electronics, University of BordjBouArréridj, Algeria. He has published numerous journal and conference papers in the field of antennas and computational electromagnetics. His research interests include printed and cylindrical antennas, transmission lines, computational electromagnetics, integral equations, finite element methods, high-performance computing, neural networks, and fuzzy logic. He can be contacted at email: f.bouttout@univ-bba.dz.

Djellid Asma received the B.Sc. and M.Sc. degrees in Electronic Engineering from the University of M'Sila, Algeria. She is currently a lecturer and researcher with the Department of Electronics, University of M'Sila, Algeria. She has co-authored several publications and actively participated in both national and international conferences. Her research interests include antennas and propagation, metamaterial-based structures, microstrip filters, and communication systems. She can be contacted at email: asma.djellid@univ-msila.dz.